PHYSICAL REVIEW D VOLUME 20, NUMBER 7 1 OCTOBER 1979

p-p resonances: A link between nuclear and hadronic excitations

Malcolm H. Mac Gregor
Lawrence Livermore Laboratory, Livermore, California 94550
(Received 26 March 1979; revised manuscript received 12 June 1979)

Evidence of resonant behavior has recently been discovered in p-p scattering, and possibly also in n-p scattering. In particular, the p-p data indicate the existence of $^1D_2$, $^3F_3$, and $^1G_4$ resonances at energies of approximately 2140, 2260, and 2430 MeV. The correlation between increasing l values and increasing energies that is observed in these resonances suggests a form of rotational motion. Since a virtually bound nucleon-nucleon state represents the low-mass limit of a multinucleon (nuclear) system, we logically expect the rotational behavior of this dinucleon state to follow the known systematics of nuclear physics. The rotational motion is highly nonadiabatic for this very light dinucleon system, so that an $l(l+1)$ energy interval rule is expected to apply, where l is the orbital angular momentum quantum number. In support of this idea, we show experimental data plots which reveal that (1) rotational bands in very light nuclei and in the dinucleon follow the expected $l(l+1)$ interval rule, and (2) the experimental moments of inertia of the rotating bandheads exhibit the expected $A^{5/3}$ behavior, where A is the atomic weight. We can extend these concepts even farther by formally sorting the observed baryon and meson resonances into nonadiabatic rotational bands. When we do this, we discover that the experimental moments of inertia of these hadron rotational bands, plotted as a function of the bandhead masses, extrapolate smoothly into the moments of inertia of the very light atomic nuclei. Applying the $l(l+1)$ energy interval rule to the observed $^1D_2$, $^3F_3$, and $^1G_4$ p-p resonances, and then extrapolating to $l=0$ to obtain the mass of the unobserved p-p bandhead, we discover that it corresponds to a virtual $pp\pi$ bound state, which is a characteristic hadronic excitation. Hence the p-p resonances form a direct and unique experimental link between nuclear and hadronic excitations: *The p-p rotational levels, which are nuclear in origin, can be used to pinpoint the mass of the p-p bandhead excitation, which is hadronic in origin.* The C_{LL}, $\Delta\sigma_L$, and $\Delta\sigma_T$ measurements carried out at Argonne are crucial in the identification of these rather weak p-p resonances. Unfortunately, the low-energy limit of these Argonne measurements falls above the predicted energy values of the (unobserved) $l=0$ and $l=1$ levels in the p-p rotational band. Thus the present results suggest the usefulness of extending the C_{LL}, $\Delta\sigma_L$, and $\Delta\sigma_T$ experiments at Argonne from the present lower limit of 1.0 GeV/c down to at least 0.8 GeV/c.

I. INTRODUCTION

In a recent paper,[1] Auer *et al.* have reported the possible existence of $^1D_2$, $^3F_3$, and $^1G_4$ proton-proton dibaryon resonances at energies of approximately 2140, 2260, and 2430 MeV. These resonance energies correspond to the positions of dips in the elastic C_{LL} spin-correlation data.[1] Other evidence for this p-p resonant structure is obtained from cross-section differences between parallel and antiparallel longitudinal ($\Delta\sigma_L$) and transverse ($\Delta\sigma_T$) total cross sections, and from Legendre expansions of differential cross section and polarization data. The central dip in the C_{LL} data was first identified as a $^3F_3$ dibaryon resonance by Hidaka *et al.*,[2] who determined its mass and width as $M=2260$ MeV, $\Gamma=200$ MeV. Some evidence of structure has also been observed in the isotopic spin $I=0$ amplitudes in neutron-proton scattering,[3,4] and it is supported by other data anomalies[5] which suggest the existence of $I=0$ dibaryon resonance behavior.

Experimentally, the discovery of this nucleon-nucleon structure was somewhat unexpected, because phase-shift analyses of lower-energy p-p and n-p elastic scattering data[6] failed to reveal any evidence of dibaryon resonance behavior. This suggests that the somewhat-higher-energy Argonne p-p and n-p experiments[1,4] are above some kind of critical threshold for resonance formation. Hence the challenging theoretical task is to determine the exact nature of these p-p resonances, and thereby ascertain the nature of the threshold which has been crossed. As we will discover, this threshold for p-p resonance formation is in fact just the pion-production threshold itself. Specifically, the occurrence of orbital angular momentum $l=2$, 3, and 4 p-p resonances at successively increasing energies indicates that we are observing a nuclear-physics type of nonadiabatic rotational band[7]; an extrapolation to $l=0$ shows that the (unobserved) rotational bandhead is a mass-shell (zero binding energy) $pp\pi$ virtual bound state.

It should be emphasized here that the theoretical analysis of these dibaryon data anomalies[1-5] is a difficult task. The experimental measurements are in the energy region that is above the inelastic pion-production threshold, and the presence of inelastic channels makes it difficult to carry out any kind of a definitive phase-shift analysis,[8] since

assumptions must be made about the inelasticity. In fact, this difficulty with the inelastic p-p and n-p phase-shift analyses furnishes part of the motivation for the present paper: By interpreting these p-p resonances as members of a rotational band, we are in a sense circumventing the difficulties that are inherent in carrying out a nucleon-nucleon phase-shift analysis when inelastic channels are open.[8]

In Sec. II of the paper we examine the behavior of nonadiabatic rotational bands in light atomic nuclei, which is an important topic that has not been sufficiently recognized, and we also study the baryon and meson resonances from this same phenomenological viewpoint. Then in Sec. III we discuss the p-p and n-p resonances, and demonstrate how they accurately bridge the gap between the nuclear and hadronic domains. As we will see, the observed p-p resonances have the following properties: (1) They obey an accurate $l(l+1)$ or $j(j+1)$ mass interval rule, (2) they have a moment of inertia that is consistent with the moments of inertia of neighboring nonadiabatic rotational bands, and (3) the mass-shell $pp\pi$ bandhead excitation is closely analogous to the excitations that are observed in other dibaryon systems. Our emphasis in this discussion is on the systematics of the experimental data, and the main content of the presentation is contained in a series of graphical displays of the data.

II. NUCLEAR AND HADRONIC NONADIABATIC ROTATIONAL BANDS

The concept of *nonadiabatic* rotational bands is essential for a proper understanding of the phenomenology of the p-p resonances. Theoretically, we can determine the nature of nonadiabatic[9,10] rotations by studying the rotational Hamiltonian[11]

$$H=(\hbar^2/2I)\hat{L}^2, \tag{1}$$

where $\hat{L}$ is the angular momentum operator and I is the effective moment of inertia. It is customary[10-13] to write

$$\hat{L}=\hat{J}-\hat{S}, \tag{2}$$

where $\hat{J}$ and $\hat{S}$ are the total angular momentum and spin angular momentum operators. Thus the rotational energy is given (schematically) by the expectation value of the operator

$$\hat{L}^2=(\hat{J}-\hat{S})^2=\hat{J}^2+\hat{S}^2-2\hat{J}\cdot\hat{S}. \tag{3}$$

The usefulness of this representation lies in the fact that the "Coriolis term" $\hat{J}\cdot\hat{S}$ tends to vanish if the rotating system satisfies the following conditions:

(A) the system is markedly aspherical, so that the rotational axes are clearly delineated;

(B) the rotational velocity is "slow" (the adiabatic[9,10] approximation), so that the rotation does not appreciably affect the intrinsic structure; and

(C) the intrinsic spin $\vec{S}$ does not have the value $\frac{1}{2}$.

Conditions (A) and (B), which are not independent of one another, combine to make it a valid approximation to write the wave function as a product of total angular momentum and intrinsic spin components.[14] Once conditions (A) and (B) are satisfied, a direct calculation using the product wave function shows[15] that the Coriolis coupling vanishes unless $\vec{S}=\frac{1}{2}$. If the Coriolis term vanishes, then the rotational energies will, from Eq. (3), follow a $j(j+1)$ interval relationship:

$$E(j)=E_0+(\hbar^2/2I)j(j+1)$$
$$\equiv E_0+E_{\rm rot}j(j+1), \tag{4}$$

where E_0 is the bandhead energy and I is the effective moment of inertia. There are many nuclei that satisfy these three conditions, and their associated rotational spectra quite accurately follow the $j(j+1)$ energy interval rule. However, near closed shells, where condition (A) fails, and for nuclei with $\vec{S}=\frac{1}{2}$, where condition (C) fails, the simple $j(j+1)$ interval rule no longer obtains.[16]

In the case of *light* atomic nuclei, where the small masses lead to rapid rotations, condition (B) is violated. Also, the broad widths of some of the low-mass rotational levels indicate that these levels last for very brief periods of time,[17] so that the rotational motion [condition (A)] is not well defined. Thus the $\hat{J}\cdot\hat{S}$ Coriolis term does *not* vanish for rotational levels in very light nuclei, which means that the rotational energies of these nuclei depend essentially just on the orbital angular momentum quantum number l, and are given by the equation

$$E(l)=E_0+(\hbar^2/2I)l(l+1)$$
$$\equiv E_0+E_{\rm rot}l(l+1). \tag{5}$$

The $^1D_2$, $^3F_3$, and $^1G_4$ p-p resonances that have been observed[1] are all $l=j$ enhancements, so that for this special case, Eqs. (4) and (5) reduce to the same equation. However, in general, this special case does not occur in the neighboring nuclear and hadronic excitations, and it is important that we use Eq. (5) rather than Eq. (4) for the intercomparison of these low-mass rotational bands.

Let us now investigate the nonadiabatic nature of the rotations in light atomic nuclei. There are two steps to this process: (a) We first determine the manner in which the moment of inertia I of a nucleus varies systematically as a function of the angular momentum of the nucleus, (2) We then use

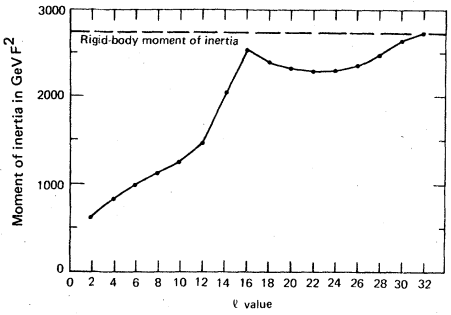

FIG. 1. The moments of inertia of the yrast levels in ^{158}Er (Ref. 18). For small l values, the moment of inertia *increases* with increasing l. This same behavior can be observed in the somewhat-more-rigid light nuclei of Figs. 2–9, and it is essential for the delineation of the nonadiabatic nature of the rotations in these light nuclei, as is shown in Figs. 6, 7, and 9.

this moment of inertia versus angular momentum criterion to deduce whether Eq. (4) or Eq. (5) is correct in a particular case. It turns out that Eq. (5), the nonadiabatic equation, is the correct one to use for all nuclei with $A \leq 20$.

In order to determine the manner in which the moment of inertia of a nucleus varies with angular momentum, we initially restrict ourselves to even-even nuclei that have $l = j$, so that we avoid the Eq. (4) versus Eq. (5) controversy. In these even-even nuclei, the "yrast" levels are defined as the lowest-energy levels at which given spin values are observed, and the $l = 0, 2, 4, \ldots$ sequence of low-spin yrast levels constitutes the ground-state rotational band. Figure 1 shows the experimental[18] moments of inertia of the yrast levels for one of the best-studied rare-earth nuclei, ^{158}Er. As can be seen in Fig. 1, the experimental moments of inertia increase steadily with increasing l values, then exhibit a sudden large increase in the "backbending" region near $l = 14$ and finally level off at just about the rigid-body value near $l = 32$. Our interest in the ^{158}Er nucleus centers on the monotonically increasing $I(l)$ behavior for small l values. This moment-of-inertia behavior indicates that heavy atomic nuclei are somewhat "spongy," at least for small l values, so that their shapes become more oblate as the angular momentum is increased.[19]

Figure 2 shows the experimental[20] yrast bands

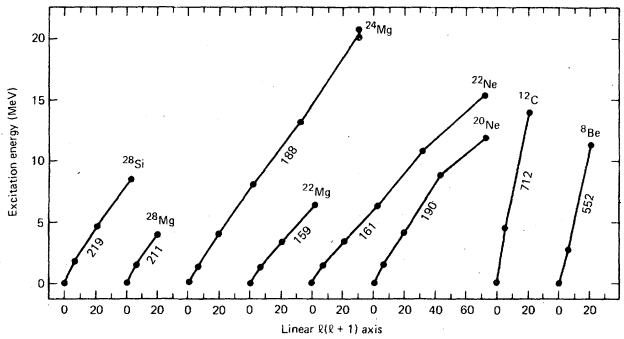

FIG. 2. Rotational excitation energies for the ground-state yrast bands of a series of light even-even nuclei (Ref. 20). As can be seen, the slopes of these yrast curves initially *decrease* slightly, showing that the moments of inertia initially *increase*, in agreement with the results of Fig. 1. The numerical value that is associated with each yrast band in Fig. 2 is the experimental value for $E_{\rm rot}$ in keV [Eq. (5)], as obtained by taking an $l(l+1)$-weighted average over the levels in the band.

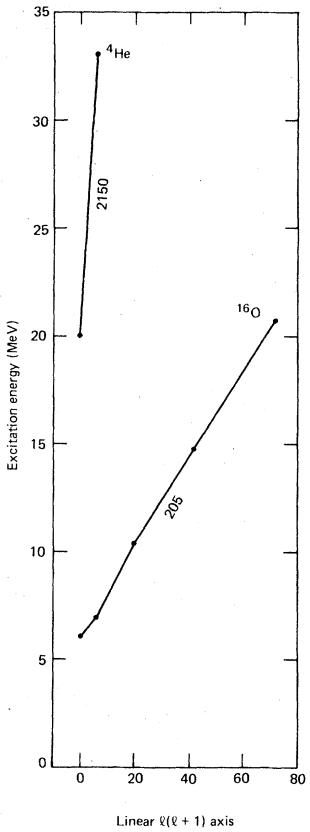

FIG. 3. "Excited-state" yrast rotational bands in ^{4}He and ^{16}O. The "doubly magic" nuclei ^{4}He and ^{16}O are spherical in shape, and hence do not have ground-state yrast rotational bands. However, they each have a deformed $J^P = 0^+$ excited-state level that serves as a rotational bandhead and combines with the usual 2^+, 4^+, $\cdots$ yrast levels to form an "excited-state yrast rotational band." The $E_{\rm rot}$ values for these two excited-state yrast bands accurately match the $A^{-5/3}$ scaling law of Eq. (6), as is demonstrated in Fig. 11. This indicates that the excited-state $J^P = 0^+$ bandheads in ^{4}He and ^{16}O have similarly deformed geometries.

for a series of light even-even nuclei, where the rotational energies of the levels are plotted against a linear $l(l+1)$ axis. As can be seen in Fig. 2, the slopes of these curves initially decrease slightly, which indicates that the moments of inertia are increasing slightly. Thus we see the same tendency towards oblateness in these light nuclei as was seen in the heavy ^{158}Er nucleus of Fig. 1, although the light nuclei are somewhat "stiffer" than ^{158}Er, since they contain fewer nucleons. Hence we have as a general (and very plausible) result that the moment of inertia of a rotating nucleus initially *increases* with increasing angular momentum. This is the criterion that we need in order to determine whether or not a given nuclear rotational motion is nonadiabatic.

Before investigating the adiabatic question, we first give two examples of specialized types of nuclear rotational bands, and we write down a scaling law for rotational energies. Figure 3 shows rotational bands in the "doubly magic" nuclei ^{4}He and ^{16}O. These nuclei are spherical in shape[21] and thus do not have ground-state rotational bands [condition (A) above]. However, they both have "excited-state" yrast bands, in which the $J^P = 0^+$ bandhead is an excited state (which is evidently deformed), and the $J^P = 2^+$ and higher states are the usual yrast levels.

Figure 4 shows the ground-state yrast band for ^{24}Mg (which was also shown in Fig. 2), and it shows in addition a "molecular" rotational band[22] that is formed in ^{12}C + ^{12}C collisions.[17] The moment of inertia that is associated with the molecular rotational band is about twice that of the ground-state yrast band, and it "corresponds closely with a classical estimate for two peripherally touching, but rigidly rotating, carbon nuclei."[17] The yrast band and the molecular band in ^{24}Mg are of interest here in that they constitute the limiting cases of a compact geometry (with a small moment of inertia) and an extended geometry (with a much

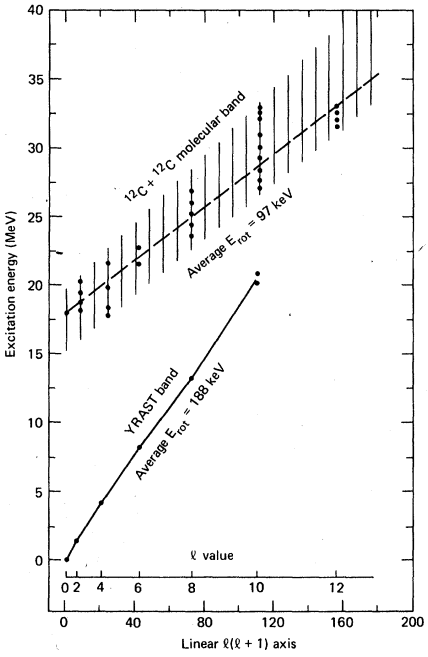

FIG. 4. The ground-state yrast rotational band in ^{24}Mg (Ref. 20), shown together with a ^{12}C + ^{12}C "molecular" rotational band in ^{24}Mg (Refs. 17 and 22). The molecular band is formed in heavy-ion collisions, and it appears in the form of a broad envelope of excitations. The moment of inertia $I = \hbar^2/2E_{rot}$ for the ^{24}Mg molecular band is about twice as large as that of the corresponding ^{24}Mg ground-state yrast band. The lower $A^{-5/3}$ scaling curve that is shown in Fig. 11 corresponds to molecular-type rotational motion in the "alpha-particle" nuclei ^{24}Mg, ^{20}Ne, ^{16}O, ^{8}Be, and ^{4}He.

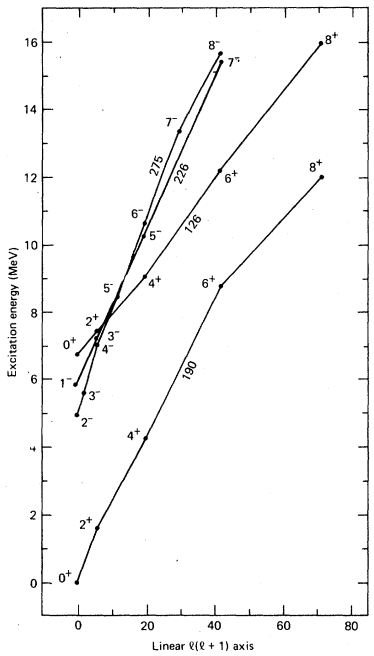

FIG. 5. Four separate rotational bands that have been identified in ^{20}Ne (Ref. 25). The ground-state 0^+, 2^+, ··· yrast band is also shown in Fig. 2, and the excited-state 0^+, 2^+, ··· rotational band is similar to the ^{4}He and ^{16}O rotational bands shown in Fig. 3. The 1^-, 3^-, 5^-, 7^- and 2^-, 3^-, 4^-, 5^-, 6^-, 7^-, 8^- rotational bands are of special interest here in that they have $l \neq J$ and hence can be used to test the nonadiabatic nature of the rotational motion in ^{20}Ne. This test is carried out in Figs. 6 and 7. The experimental E_{rot} values for these four rotational bands vary by more than a factor of 2, but they all fit in with the $A^{-5/3}$ scaling law of Eq. (6), as is shown in Fig. 11.

larger moment of inertia). As we will see, the moments of inertia of the light nuclei all fall within these two limits.

In comparing nuclei with different atomic weights A, there is a simple scaling law that can be deduced for the rotational energies. These nuclei have masses $M \propto A$, and if they have similar shapes they have effective radii $R \propto A^{1/3}$. Thus the rotational energy parameter $E_{\rm rot}$ of Eqs. (4) and (5) scales as

$$E_{\rm rot} \equiv \hbar^2/2I \propto 1/I \propto 1/MR^2 \propto A^{-5/3}. \qquad (6)$$

Examples of this $A^{-5/3}$ scaling law are exhibited by the ^{4}He, ^{16}O, and ^{24}Mg rotational bands of Figs. 3 and 4. The ratio of the experimental $E_{\rm rot}$ values for the ^{4}He and ^{16}O nuclei of Fig. 3 is 10.5, which is in good agreement with their $A^{-5/3}$ ratio of 10.1. Also, the ratio of the experimental $E_{\rm rot}$ values for ^{16}O (Fig. 3) and "molecular" ^{24}Mg (Fig. 4) is 2.1, which is in good agreement with their $A^{-5/3}$ ratio of 2.0. The fact that these ^{4}He, ^{16}O, and ^{24}Mg nuclei follow the $A^{-5/3}$ scaling law of Eq. (6) indicates that all three of these nuclei have similar (molecular-type) geometries. By way of contrast, the ratio of the experimental $E_{\rm rot}$ values for ^{12}C (Fig. 2) and ^{16}O (Fig. 3) is 3.5, which is not in agreement with their $A^{-5/3}$ ratio of 1.6. This disagreement is due to the fact that the ^{12}C nucleus, in contrast to the expanded molecular geometry of the ^{16}O nucleus, has a compact prolate shape[23,24] with respect to rotations.

We now come to the question of determining how small the atomic weight A must be for a nuclear rotational band to be regarded as nonadiabatic. We can answer this question by studying the ^{20}Ne nucleus, which has four identified rotational bands.[25] These rotational bands are shown in Fig. 5. In addition to its ground-state $0^+, 2^+, 4^+, 6^+, 8^+$ yrast band (which is also shown in Fig. 2), ^{20}Ne has an excited-state $0^+, 2^+, 4^+, 6^+, 8^+$ rotational band that is closely analogous to the rotational bands shown in Fig. 3. Both of these rotational bands, which contain $l=j$ excitations, show the initially decreasing slopes (initially increasing moments of inertia) that we expect to find on the basis of the results displayed in Figs. 1 and 2. The other two rotational bands in ^{20}Ne contain levels that are not $l=j$ excitations, so that these two rotational bands can be used to investigate the nonadiabaticity of

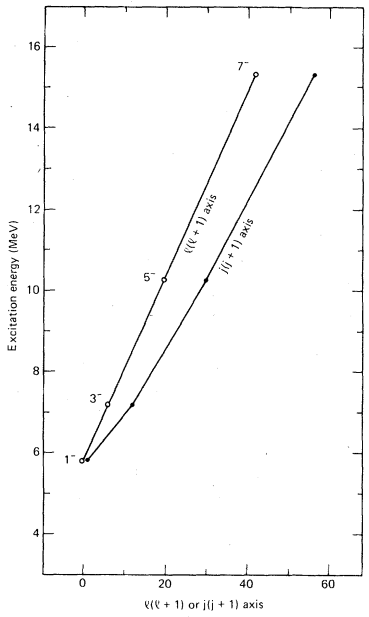

FIG. 6. The $J^P = 1^-, 3^-, 5^-, 7^-$, rotational band in ^{20}Ne, plotted against both $j(j+1)$ and $l(l+1)$ axes. The $l(l+1)$ plot is linear, but the $j(j+1)$ plot shows an initially *increasing* slope with increasing spin value, which is just the opposite of the behavior that is demonstrated in the $l=J$ curves of Figs. 1 and 2. Hence the $l(l+1)$ plot is singled out experimentally as being physically significant. This indicates that the rotational motion is nonadiabatic, and is governed by Eq. (5). Figures 7 and 9 substantiate this result. Thus we can conclude that for atomic nuclei with $A \leq 20$, the rotational motion is nonadiabatic, so that the rotational energies depend just on the orbital angular momentum l, and not on the total angular momentum J.

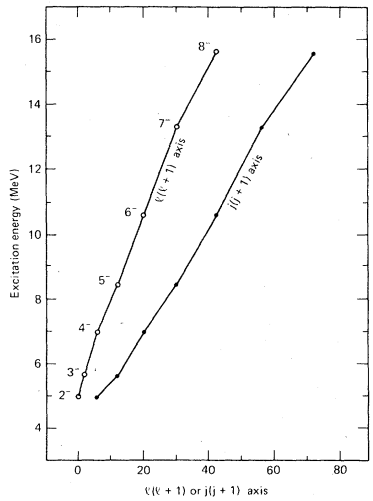

FIG. 7. The $J^P = 2^-, 3^-, 4^-, 5^-, 6^-, 7^-, 8^-$ rotational band in ^{20}Ne, plotted against both $j(j+1)$ and $l(l+1)$ axes. The $l(l+1)$ plot shows an initially *decreasing* slope, in agreement with Figs. 1 and 2, but the $j(j+1)$ plot shows an initially *increasing* slope. Hence the $l(l+1)$ plot is singled out experimentally as being physically significant, which indicates that the rotational motion is nonadiabatic, in line with the results of Fig. 6.

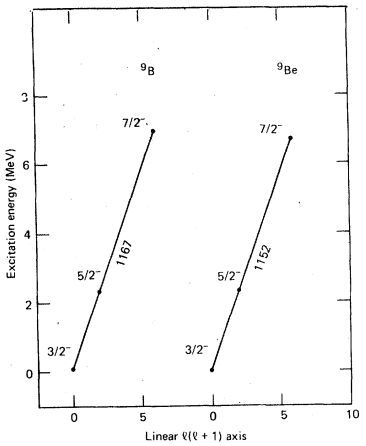

FIG. 8. Rotational bands in ^{9}B and ^{9}Be. These are examples of rotational bands that have half-integral spins. In Fig. 9, the rotational motions of these light nuclei are shown to be nonadiabatic. The $E_{\rm rot}$ values of 1167 and 1152 keV for these two rotational bands fit in with the $A^{-5/3}$ scaling law of Eq. (6), as is demonstrated in Fig. 11.

the rotational motion. Figure 6 shows the $1^-, 3^-, 5^-, 7^-$ rotational band in ^{20}Ne plotted against both an $l(l+1)$ and a $j(j+1)$ abscissa. As can be seen in Fig. 6, the $l(l+1)$ plot has the correct shape (an initially decreasing slope), but the $j(j+1)$ plot does not. Thus the $l(l+1)$ plot is singled out experimentally as being correct. Figure 7 shows similar plots for the $2^-, 3^-, 4^-, 5^-, 6^-, 7^-, 8^-$ rotational band in ^{20}Ne, and again the $l(l+1)$ plot is singled out experimentally as being correct. Thus we have the empirical result that the nuclear rotational bands in ^{20}Ne are nonadiabatic.

Figure 8 shows matching rotational bands in ^{9}B and ^{9}Be that feature half-integral spins. The very large value for the rotational energy parameter in each of these light nuclei, $E_{\rm rot} > 1$ MeV, indicates directly that the rotations are highly nonadiabatic. This result is confirmed in Fig. 9, which shows the ^{9}B and ^{9}Be rotational bands of Fig. 8 plotted against both $l(l+1)$ and $j(j+1)$ abscissas. As can be seen in Fig. 9, the $l(l+1)$ plots exhibit the correct behavior (initially decreasing slopes), whereas the $j(j+1)$ plots are physically incorrect.

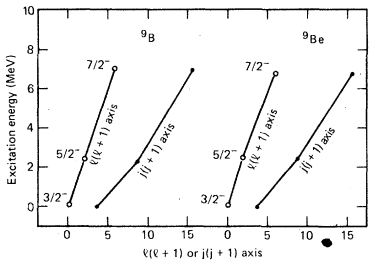

FIG. 9. The ^{9}B and ^{9}Be $J^P = \frac{3}{2}^-, \frac{5}{2}^-$, and $\frac{7}{2}^-$ rotational bands of Fig. 8 plotted against both $j(j+1)$ and $l(l+1)$ axes. The $l(l+1)$ plots show initially constant or decreasing slopes, whereas the $j(j+1)$ plots show initially increasing (and therefore physically incorrect) slopes. Thus, just as in Figs. 6 and 7, the $l(l+1)$ plots are singled out experimentally as being correct, which is a consequence of the nonadiabatic nature of the rotations.

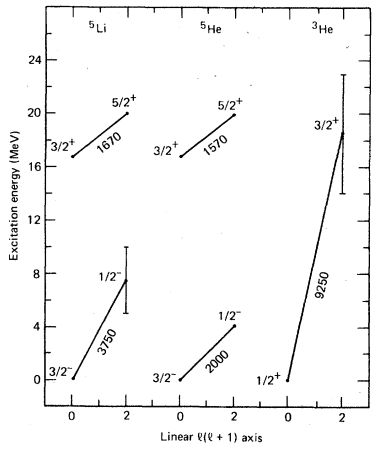

FIG. 10. Fragmentary and highly nonadiabatic rotational bands in very light atomic nuclei. The $J^P = \frac{3}{2}^-, \frac{5}{2}^-$ rotational bands in ^{5}Li and ^{5}He are similar to the ^{9}B and ^{9}Be rotational bands shown in Fig. 8. However, the $J^P = \frac{1}{2}^-$ rotational levels in ^{5}Li and ^{5}He represent rotations in which the orbital angular momentum vector is oriented in the opposite direction to that of the spin vector; three reasons are given in the text for believing that these are in fact rotational excitations. The evidence for the existence of the $J^P = \frac{3}{2}^+$ level in ^{3}He is controversial, but it does exist (Refs. 27–30). As is shown in Fig. 11, the $E_{\rm rot}$ values for these rotational bands follow the $A^{-5/3}$ scaling law established by the heavier nuclei, and they serve to delineate the value of $E_{\rm rot}$ that is anticipated for the even lighter p-p dibaryon rotational band (see Fig. 20).

From the results that are displayed in Figs. 6, 7, and 9, we can conclude that all nuclei with $A \leq 20$ have nonadiabatic rotational modes, so that their rotational energies depend just on the orbital angular momentum l. Hence Eq. (5) is the correct rotational energy equation to use for all nuclei with atomic weight $A \leq 20$. Furthermore, since baryon and meson resonances[26] are quantized in the same multiples of $j\hbar$ or $l\hbar$ as are light atomic nuclei, and since they have masses that are comparable to $A = 1$–3, they must also correspond to highly nonadiabatic rotations.

The final examples of nonadiabatic rotational bands in light nuclei are shown in Fig. 10. These include two rotational bands each in ^{5}Li and ^{5}He,

and one somewhat speculative rotational band in ^{3}He. Due to the highly nonadiabatic nature of the rotations for these very light nuclei, only two levels exist in each rotational band. The $J^P = \frac{3}{2}^+, \frac{5}{2}^+$ rotational bands in ^{5}Li and ^{5}He are straightforward extensions of examples we have studied above. However, the $J^P = \frac{3}{2}^-, \frac{1}{2}^-$ rotational bands in ^{5}Li and ^{5}He represent $l = 0$ and $l = 1$ states, respectively, of a spin $S = \frac{3}{2}$ nucleus, with the orbital angular momentum $l = 1$ in the $J = \frac{1}{2}$ levels being oriented opposite to the spin direction. We have three reasons for identifying the $J = \frac{1}{2}$ levels in ^{5}Li and ^{5}He as rotational excitations: (1) The very broad widths of these resonances correspond to the broad widths of the other rotational levels in very light nuclei. (2) The experimental values of $E_{\rm rot}$ for these rotational bands follow the $A^{-5/3}$ scaling law of Eq. (6) (see Fig. 11). (3) The values of $E_{\rm rot}$ are in agreement with estimates based on the classical P wave ($l = 1$) rotation of α, p (^{5}Li) and α, n (^{5}He) dumbbells.[23]

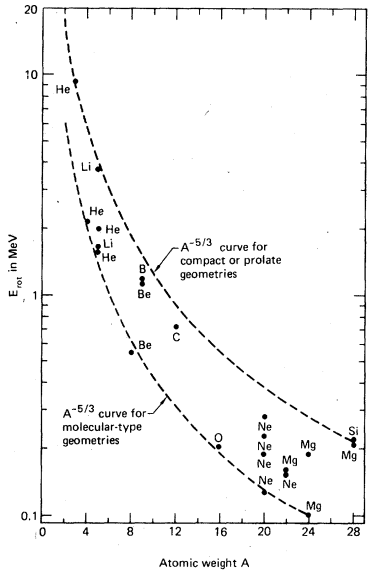

FIG. 11. Experimental values of the rotational energy parameter $E_{\rm rot}$ [see Eq. (5)] for the nonadiabatic rotational bands of Figs. 2–5, 8, and 10, plotted as a function of the atomic weight A of the rotating bandhead. The lower and upper $A^{-5/3}$ scaling curves [see Eq. (6)] shown in Fig. 11 correspond to spread-out molecular-type geometries, and to very compact or prolate geometries, respectively. As can be seen in Fig. 11, all of the experimental $E_{\rm rot}$ values fall within two limits. By extrapolating these results to the value $A = 2$, we estimate that the p-p dibaryon rotational band must have an $E_{\rm rot}$ value of 6 to about 18 MeV. The experimental p-p values, as obtained from Fig. 20, is 20.6 MeV, which indicates that the rotating p-p bandhead has a very compact geometry. This is perhaps in line with the fact that the p-p dibaryon excitation energy of about 140 MeV (Fig. 20) represents a characteristic hadronic (strong) excitation (see Fig. 21), rather than a relatively weak nuclear-type excitation

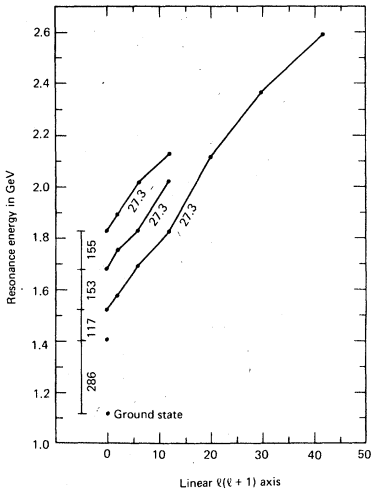

FIG. 12. The identified Λ resonances (Ref. 26), grouped into nonadiabatic rotational bands (Refs. 31–33) and plotted against an $l(l+1)$ abscissa. The spacing of the $l = 0$ bandheads is roughly comparable to the $\pi \sim 140$ MeV excitation energy that is observed in the p-p rotational band (Fig. 20). The experimental rotational energies $E_{\rm rot} = 27.3$ MeV for these Λ rotational bands are somewhat larger than the $E_{\rm rot}$ values shown in Fig. 11.

The $J^P = \frac{1}{2}^+, \frac{3}{2}^+$ rotational band in ^{3}He shown in

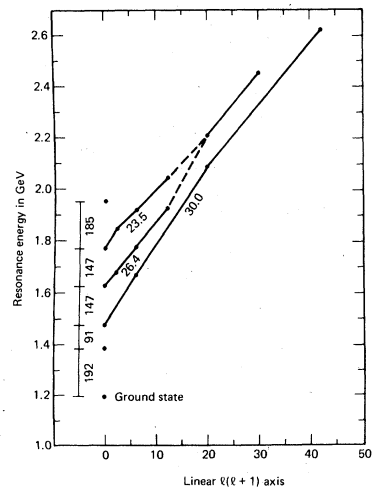

FIG. 13. The identified Σ resonances (Ref. 26), grouped into nonadiabatic rotational bands (Refs. 31–33). These Σ rotational bands are similar to the Λ rotational bands of Fig. 12, although they are not as complete. Two very broad G and H ($l = 4$ and 5) Σ resonances may reflect contributions from more than one rotational band, as is indicated by the dotted lines in the figure.

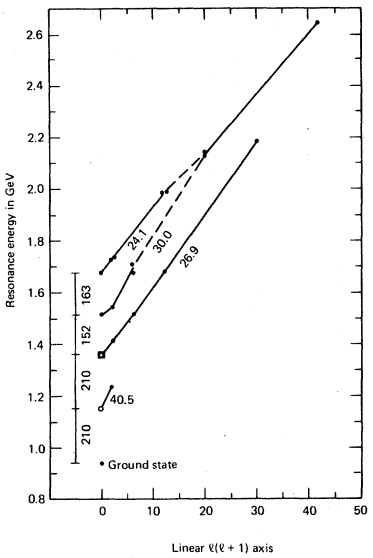

FIG. 14. The identified N resonances (Ref. 26), grouped into nonadiabatic rotational bands (Refs. 31–33). Open circles denote unobserved S-state bandheads. However, the open circle enclosed in a square denotes a bandhead that was predicted many years ago (Ref. 31) and which has just recently been discovered (Ref. 34).

Fig. 10 is the lightest of the nuclear rotational bands. The experimental evidence[27] with respect to the $J^P = \frac{3}{2}^+$ state in ^{3}He is somewhat unclear. Whereas some experiments show evidence of resonance behavior, others do not.[27,28] However, a number of experiments[28-30] give indications of a resonance somewhere between 14 and 23 MeV, and a phase-shift analysis indicates that this enhancement corresponds to a $J = \frac{3}{2}$ P wave.[30] Thus we have shown this state in Fig. 10 at an energy halfway between 14 and 23 MeV and with an experimental error of ±4.5 MeV in the position of the resonance. As we will see in Fig. 11, this assignment yields a value $E_{\text{rot}} = 9.25$ MeV that accurately

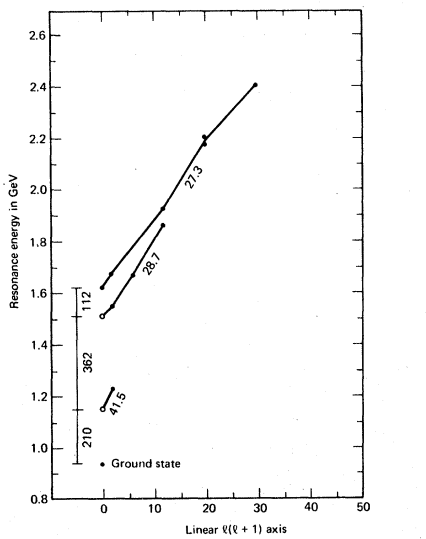

FIG. 15. The identified Δ resonances (Ref. 26), grouped into nonadiabatic rotational bands (Ref. 31–33). Open circles denote unobserved S-state bandheads. It should be noted here that $j(j+1)$ plots rather than $l(l+1)$ plots do not yield phenomenologically useful baryon rotational bands; this result is sufficient to indicate the nonadiabatic nature of these baryon rotations.

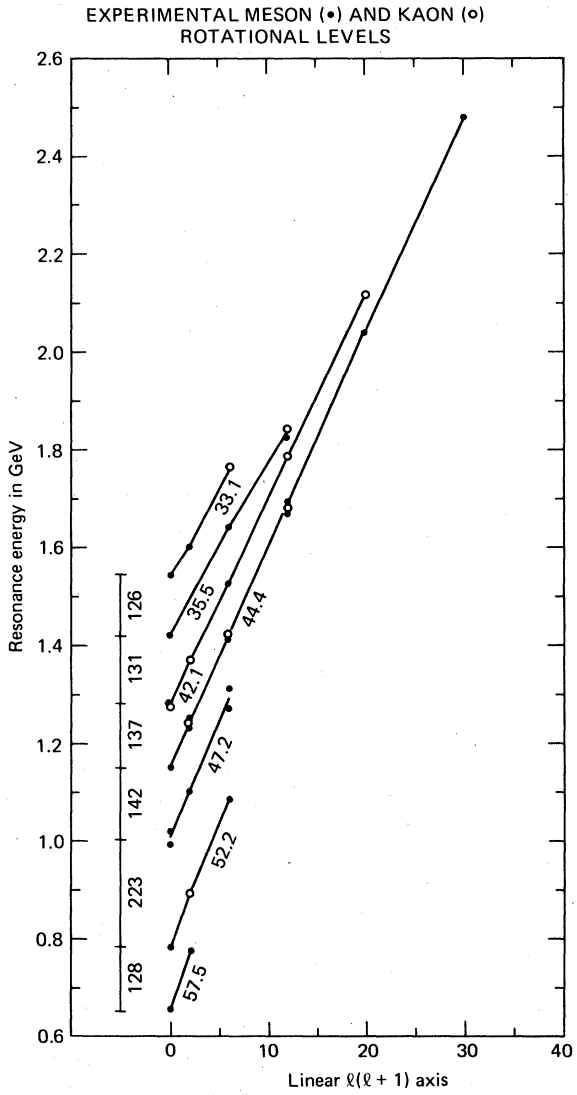

FIG. 16. The identified broad-width ($\Gamma > 50$ MeV) meson and kaon resonances (Ref. 26), grouped into nonadiabatic rotational bands (Refs. 32 and 33). The bandhead locations correspond to narrow-width ($\Gamma < 50$ MeV) resonances, and they characteristically appear at 140 MeV intervals. Since the meson bandheads are lighter than the baryon bandheads of Figs. 12–15, the meson E_{rot} values are correspondingly larger (see Fig. 17).

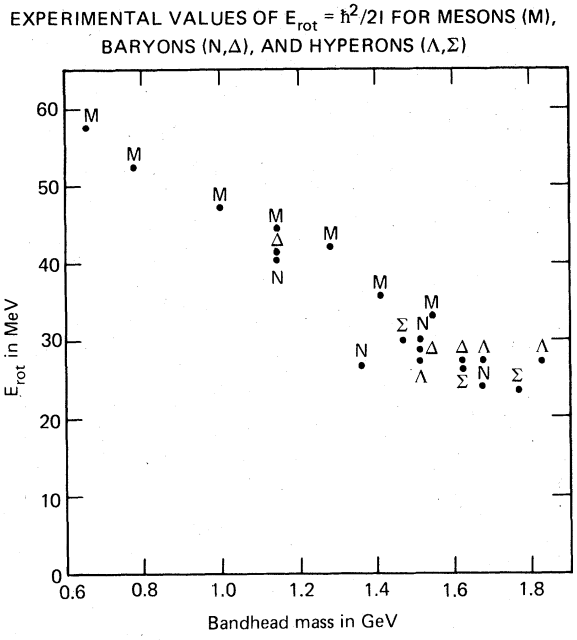

FIG. 17. The experimental values of E_{rot} [Eq. (5)] for the hyperon, baryon, and meson rotational bands of Figs. 12–16, plotted as a function of the mass of the bandhead excitation. In Fig. 18, these *hadronic* values of E_{rot} are combined together with the *nuclear* values of E_{rot} from Fig. 11.

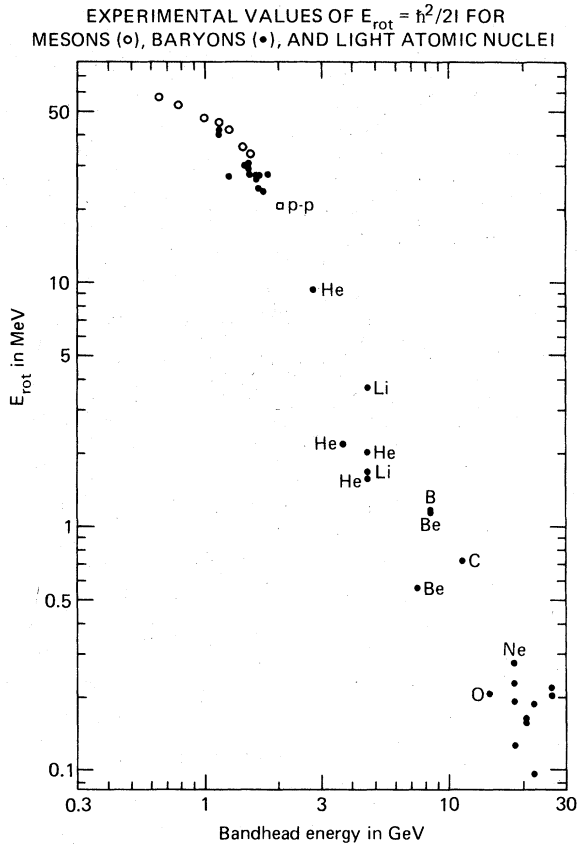

FIG. 18. Experimental values of E_{rot} for the hadronic rotational bands of Fig. 17 and the nuclear rotational bands of Fig. 11, plotted together as a function of the mass of the bandhead. Also shown is the value of E_{rot} for the p-p rotational band of Fig. 20. As can be seen in Fig. 18, the E_{rot} values for these radically different systems combine together to form a uniform curve that varies as a monotonic function of the bandhead mass. However, the $A^{-5/3}$ scaling law [Eq. (6)] that is obeyed by the nuclear rotational bands (see Fig. 11) is not continued into the hadronic rotational bands; the hadronic values of E_{rot} show a much weaker dependence on the mass of the bandhead, which indicates that the hadronic bandhead "geometries" do not vary as the cube root of the mass.

matches the $A^{-5/3}$ scaling of the E_{rot} values for the other light nuclei. This ^{3}He E_{rot} value also matches an estimate based on a configuration analogous to that of the ^{12}C nucleus.[23] The nuclear levels shown in Fig. 10 plus the ^{4}He levels shown in Fig. 3 represent the lightest and therefore the most nonadiabatic of the nuclear rotational bands; hence they are of decisive importance in helping us to interpret the rotational motion that is observed[1] in the even lighter p-p dibaryon system.

Having discussed these nuclear rotational bands separately, it is important that we now combine them together to see how they intercompare. This is accomplished in Fig. 11, which displays the E_{rot} values for all of the rotational bands shown in Figs. 2–5, 8, and 10 plotted as a function of the atomic weight A. [The E_{rot} value that is quoted for each rotational band in these figures is an $I(I+1)$-weighted average over the experimental E_{rot} values for the individual levels in the band.] Also shown in Fig. 11 are two $A^{-5/3}$ curves that are based on Eq. (6). The lower $A^{-5/3}$ curve corresponds to the "molecular-type" rotational bands, and, as can be seen in Fig. 11, the ^{24}Mg, ^{16}O, ^{8}Be and ^{4}He molecular bands have E_{rot} values that lie right along this curve. The upper $A^{-5/3}$ curve corresponds, roughly speaking, to very compact and in some cases prolate nuclear configurations. As is shown in Fig. 11, these two $A^{-5/3}$ curves serve as an envelope that encompasses the E_{rot} values for all of the nonadiabatic rotational bands in very light atomic nuclei.

By extrapolating the two $A^{-5/3}$ curves in Fig. 11 to the value $A = 2$, we can estimate the the p-p dinucleon system must have a rotational energy parameter E_{rot} that lies somewhere between 6 and about 18 MeV. As we will see in Sec. III, the upper value of 18 MeV is approximately correct (which shows that the hadronically bound p-p dinucleon state has a very compact geometry). However, before discussing the dinucleon system in detail,

we first consider the rotational bands that can be constructed from the measured[26] baryon and meson resonances, since these hadron rotational bands serve to further delimit the moment-of-inertia value that we expect to find for the p-p system. The key point to keep in mind with respect to this investigation is the *nonadiabatic* nature of the rotational motion, which makes Eq. (5) the overriding rotational energy equation for all light (<20 GeV/c^2) rotating systems, regardless of their internal quantum numbers.

It is possible to formally group the identified[26] baryon and meson resonances into nonadiabatic rotational bands, using the rotational systematics of nuclear physics as a guide. In particular, Eq. (5) serves as the rotational energy equation; and Fig. 11 makes it clear that the hadron rotational bands, whose bandheads correspond to the mass region $A<2$, must have $E_{\rm rot}$ values which are somewhat larger than 20 MeV. The interesting aspect about these hadron rotational bands is that, in combination with the nuclear rotational bands of Fig. 11, they enable us to bracket the region where the $A\simeq 2$ p-p dinucleon rotational band appears. Since the systematics of these hadron rotational bands has been thoroughly documented elsewhere,[31-33] we give here only a graphical display of the results. Figure 12 shows the observed Λ resonances[26] grouped into nonadiabatic rotational bands, Fig. 13 shows the Σ resonances, Fig. 14 shows the N resonances, Fig. 15 shows the Δ resonances, and Fig. 16 shows the meson resonances. As can be seen in Figs. 14 and 15, some of the N and Δ rotational bands have missing S states (whose locations are denoted by open circles), just as the p-p rotational band has a missing S state (see Fig. 20). However, it is interesting to note that one of the missing S states, $N(1359)$, whose existence has long been predicted,[31] was just recently discovered by a Tokyo group[34] (see the location marked with a square in Fig. 14).

The experimental $E_{\rm rot}$ values[33] that we obtain from the nonadiabatic hyperon, baryon, and meson rotational bands of Figs. 12–16 are shown plotted together in Fig. 17. As can be seen in Fig. 17, the rotational energy parameter $E_{\rm rot}$ varies inversely with the mass of the rotating bandhead, but this dependence on mass is much weaker than the $A^{-5/3}$ mass dependence shown in Fig. 11. The really interesting aspect of these studies occurs when we combine together the hadronic $E_{\rm rot}$ values of Fig. 17 with the nuclear $E_{\rm rot}$ values of Fig. 11. This result is shown in Fig. 18, where it can be seen that the $E_{\rm rot}$ values for these two disparate systems fit smoothly together, and they accurately delimit the expected $E_{\rm rot}$ value for the p-p dibaryon system. In fact, looking ahead to the results of the next section, we have included the experimental p-p $E_{\rm rot}$ value in Fig. 18, and it is just the value that is obtained by interpolating between these two domains.

As the final result in this section, we show in Fig. 19 the experimental moments of inertia that correspond to the $E_{\rm rot}$ values of Fig. 18. Again, the accurate agreement of the p-p moment of inertia with those of hadrons and of light atomic nuclei is clearly in evidence.

The hadron rotational levels that are shown in Figs. 12–16 are arranged in the order of increasing l values. It should be pointed out here that it is not possible to form similar hadron rotational bands based on increasing J values rather than increasing l values.[35] This fact is sufficient to establish the nonadiabatic nature of the hadron rotational excitations.

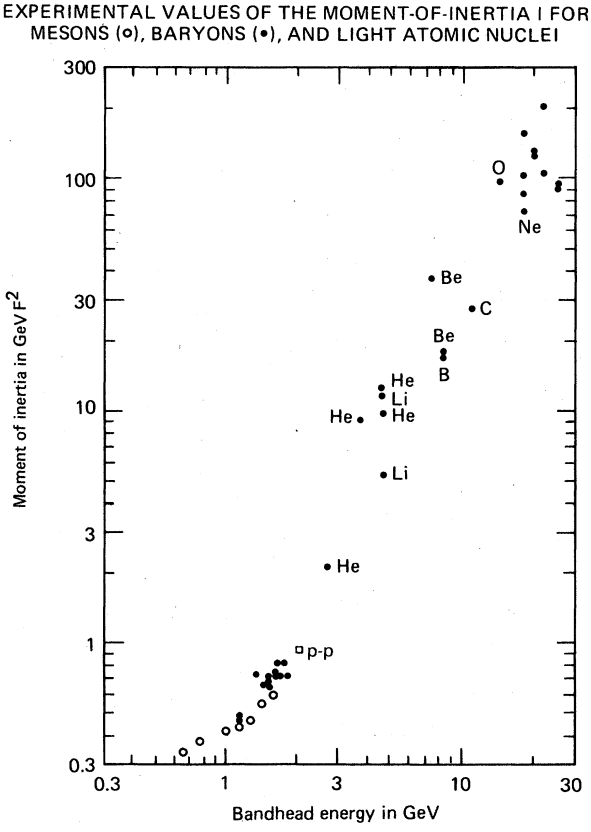

FIG. 19. Experimental values of the moments of inertia $I=\hbar^2/2E_{\rm rot}$ that correspond to the $E_{\rm rot}$ values of Fig. 18. The p-p dibaryon system stands at the boundary between the domains of nuclear and hadron physics, and the experimental p-p moment of inertia, as obtained from Fig. 20, accurately matches the values that are obtained by extrapolating from both of these domains. This suggests that the three reported p-p resonances (Ref. 1) do in fact correspond to levels in a nonadiabatic p-p dinucleon rotational band.

III. THE p-p NONADIABATIC ROTATIONAL BAND

Nucleon-nucleon scattering experiments involve the interaction of two spin-$\frac{1}{2}$ particles; this interaction has a five-dimensional complex representation in spin space. At the higher energies, many partial waves contribute to the scattering matrix. This makes the identification of N-N resonances a difficult task, since an enhancement in one particular partial wave may have only a small effect on the standard N-N "observables,"[36] which in general reflect the contributions of many partial waves.

A decade ago, nucleon-nucleon experiments in the elastic energy region (below the threshold for pion production) were complete enough that a reasonably well-defined scattering matrix could be determined,[6] and this scattering matrix showed no evidence for resonant behavior in any of the partial waves. The extension of the nucleon-nucleon scattering matrix to somewhat higher energies[8] also failed to disclose the existence of dinucleon resonances, although the results in this inelastic energy region were clearly ambiguous. Using a dispersion-relation analysis, Arndt[37] pointed out that there was possibly some evidence for resonant behavior in the $^1D_2$ phase.

Recently, an experimental breakthrough in this situation occurred at Argonne, with the simultaneous use of polarized beams and polarized targets. This makes it possible to carry out nucleon-nucleon measurements in a single spin state, which greatly magnifies the effect of a resonance if it happens to occur in that particular spin state. The first indication of anomalous nucleon-nucleon behavior was obtained from p-p measurements[38] of $\uparrow\uparrow$ and $\uparrow\downarrow$ spin states oriented perpendicular to the beam direction, which showed an unexpected enhancement in the cross section $\Delta\sigma_T = \sigma^{\rm tot}(\uparrow\downarrow) - \sigma^{\rm tot}(\uparrow\uparrow)$. This result was followed by p-p measurements[39] of $\rightrightarrows$ and $\rightleftarrows$ spin states oriented parallel to the beam direction, which exhibited a striking energy dependence in the cross section $\Delta\sigma_L = \sigma^{\rm tot}(\rightrightarrows) - \sigma^{\rm tot}(\rightleftarrows)$. Subsequent measurements[40] of the p-p spin correlation parameter C_{LL} revealed the existence of three clear-cut dips, which occur at $P_{\rm lab}$ momenta of 1.17, 1.5, and 2.0 GeV/c. The central C_{LL} dip at 1.5 GeV/c, which is the most prominent one experimentally, was identified as a $^3F_3$ dibaryon resonance by Hidaka *et al.*[2] Some evidence of structure has also been noted in the corresponding n-p amplitudes, in the form of an isotopic spin $I=0$ effect that closely resembles the $I=1$ "$^3F_3$ effect" in mass, width, and inelasticity.[3] The $\gamma+d\rightarrow p+n$ measurements of Kamae *et al.*[5] also point to the existence of anomalies in the $I=0$ amplitudes.

The topic of these possible dinucleon resonances is a very lively one at the present time, and several comprehensive summaries have been written on this subject.[4,41,42] Accordingly, we do not attempt to recapitulate all of this information here, but only the part that is relevant to the present discussion. In particular, we are mainly concerned with the determination of the masses and widths of these dinucleon anomalies and also (briefly) with the theoretical efforts that have been made to account for their existence. The *masses* of the dinucleon anomalies are important in that they give the energy interval spacings. It is clear from the results of the preceding sections that a highly nonadiabatic dinucleon rotational band must follow an $l(l+1)$ interval rule, and a crucial task is to test this prediction against the observed p-p enhancements. The significance of the *widths* of the p-p anomalies stems from the fact that, in the hadron resonances, rotationless ($l=0$) excitations characteristically have widths $\Gamma<50$ MeV, whereas rotational ($l>0$) excitations characteristically have widths $\Gamma>50$ MeV.[43] Hence if these p-p dibaryon anomalies are members of a hadronically excited rotational band, then we expect them to have widths of 50 MeV or more. The determination of the $^{2S+1}l_J$ phase-shift assignments for these anomalies has been thoroughly discussed elsewhere,[1,4,41,42] and we simply take over the conclusions of these analyses.

From a study of the results of π-N and K-N phase-shift analyses, it is clear that the occurrence of a dip in the inelastic amplitudes is a reliable indicator for determining both the existence and the position of a resonance. Although the situation is not quite the same, the occurrence of dip structure in the p-p C_{LL} data is also a significant indicator for resonance formation. The three reported C_{LL} dips[40] correspond to the p-p center-of-mass energies 2139, 2254, and 2430 MeV, respectively. Thus this C_{LL} measurement serves to delineate the energies of the three p-p anomalies. In addition, the $\Delta\sigma_T$ and $\Delta\sigma_L$ measurements mentioned above,[38,39] and also the standard p-p observables,[36] contribute information about the p-p structure in this energy region. In Table I we summarize the information about masses and widths that has been obtained from direct analyses of the data,[1,2,4] from comprehensive phase-shift analyses,[42,44] and from forward-dispersion relations.[45] Since the slightly different mass values that are obtained by various workers represent different ways of looking at more or less the same set of data, the spread in mass values shown in Table I serves as a rough measure of the inherent uncertainties in the data. The masses and widths that were deduced from these analyses[1,2,4,42,45]

TABLE I. Determinations of the masses and widths of the Argonne p-p dibaryon resonances.

Reference	Data used or method	Resonance values obtained $^1D_2$	$^3F_3$	$^1G_4$
Auer *et al.*, Ref. 1	C_{LL} dips	P_{lab} = 1.17 GeV/c	1.5 GeV/c	2.0 GeV/c
		$E_{c.m.}$ = 2139 MeV	2254 MeV	2430 MeV
Hidaka *et al.*, Ref. 2	P, $\Delta\sigma_L$		M = 2260 MeV	
			Γ = 200 MeV	
Hoshizaki, Ref. 42	Phase shifts	M = 2140–2150 MeV[a]	M = 2220 MeV	
		Γ = 50–100 MeV	Γ = 100–150 MeV	
Grein and Kroll, Ref. 45	Dispersion relation	...	M = 2320 MeV	M = 2390 MeV
			Γ = 290 MeV	Γ = 100 MeV
Yokosawa, Ref. 4	Summary paper	M = 2140–2170 MeV	M = 2200–2260 MeV	M = 2430–2500 MeV
		Γ = 50–100 MeV	Γ = 100–150 MeV	$\Gamma\sim$ 150 MeV
Values used in the present paper		M = 2140 MeV	M = 2260 MeV	M = 2430 MeV
		$\Gamma\sim$ 75 MeV	Γ = 150 MeV	$\Gamma\sim$ 100 MeV

[a] Corrected for cusp effect.

are shown at the bottom of Table I. The mass values that have been selected are essentially just those of the positions of the C_{LL} dips. The widths are significant in that they are all larger than 50 MeV, and hence are indicative of rotational excitations.[43]

The main discussion about these p-p anomalies has centered on their interpretation. Traditionally, resonant behavior is manifested by the motions that occur in Argand diagrams. In their forward-dispersion-relation analysis, Grein and Kroll[45] generated Argand plots that indicate resonant behavior for the $^3F_3$ and $^1G_4$ phases, but not for the $^1D_2$ phase. Hoshizaki[42] carried out a phase-shift analysis in which Argand plots of the $^3F_3$ and $^1D_2$ phases indicate resonant behavior. Arndt,[46] in a recent preliminary phase-shift analysis with both the real and imaginary phases searched, found evidence for $^1D_2$ resonant behavior, and perhaps some indication of a $^3F_3$ effect; however, the nucleon-nucleon data base becomes rapidly incomplete at energies above those available at LAMPF ($E_{c.m.}$ = 2240 MeV), so that a full-blown phase-shift analysis is not yet possible at the higher energies. These inherent ambiguities in the p-p data analysis have led to a great deal of discussion in the literature as to whether resonance formation is or is not occurring.[37,47-50] However, information other than Argand diagrams can be used to detect resonances. Hidaka,[41] in a detailed analysis of the p-p $^3F_3$ anomaly, lists six pieces of evidence which indicate resonant behavior: (1) the structure in $\Delta\sigma_L$, (2) a Legendre expansion of the polarization data, (3) a peak in the total elastic cross section, (4) a dip in the C_{LL} data, (5) the Grein and Kroll[45] dispersion analysis, and (6) the Hoshizaki[42] phase-shift analysis. Items (5) and (6) involve the use of Argand plots, but items (1)–(4) do not. Furthermore, Hidaka[41] points out in detail that the Argonne data in the $^3F_3$ region near 1.5 GeV/c cannot be accounted for on the basis of threshold effects, "Deck" models,[48] one-pion-exchange three-body theories,[49] or one-boson-exchange inelastic threshold models.[50] The conclusion that emerges from this analysis of the Argonne p-p data is that the $^3F_3$ anomaly, and probably also the $^1D_2$ and $^1G_4$ anomalies, are due to Breit-Wigner–type resonance formation.[1,2,4,41]

Guided by the results of the above discussion, we assume the existence of three measured p-p dibaryon resonances:

$$^1D_2(2140)\Gamma\sim 75,\quad ^3F_3(2260)\Gamma\sim 150,\quad ^1G_4(2430)\Gamma\sim 100. \tag{7}$$

This brings us face to face with the problem of accounting for these three resonances. If these resonances correspond to hadronically excited dibaryon states, then, as mentioned above, their relatively broad widths ($\Gamma > 50$ MeV) suggest that they are members of a rotational band.[43] But for this to be true, it follows from their small ($A \simeq 2$) mass values that they must obey the $l(l+1)$ energy interval rule of Eq. (5) for nonadiabatic rotations. However, since these $^1D_2$, $^3F_3$, and $^1G_4$ p-p resonances happen to be $l = J$ excitations, their behavior is the same with respect to both the nonadiabatic Eq. (5) and the adiabatic Eq. (4). Thus the nonadiabatic assumption of Eq. (5) is not, strictly speaking, necessary for the analysis of these particular p-p resonances, although the small mass of the p-p dinucleon bandhead indicates that the p-p rotational motion must in fact be highly nonadiabatic. In Fig. 20 the three p-p resonances of Eq. (7) are shown plotted against an $l(l+1)$ or $j(j+1)$ abscissa. The linearity of the curve gen-

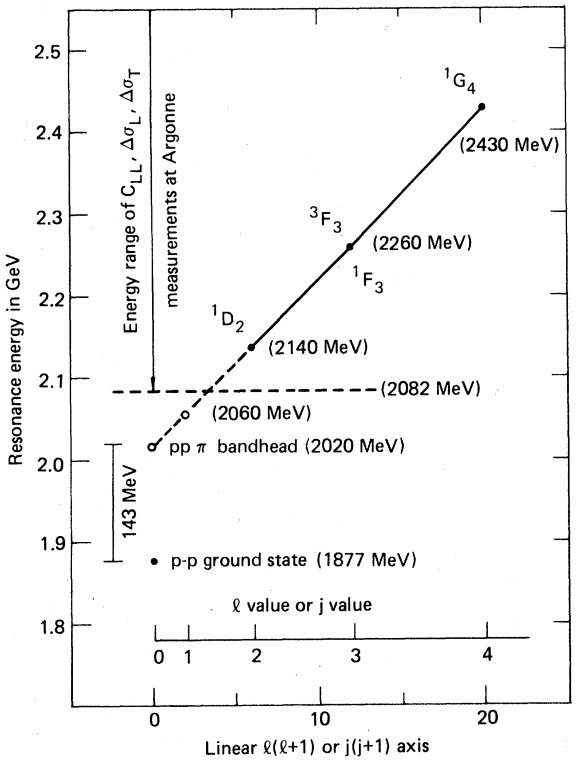

FIG. 20. The nonadiabatic dinucleon rotational band that is delineated by the p-p resonances $^1D_2(2140)\Gamma \sim 75$, $^3F_3(2260)\Gamma \sim 150$, and $^1G_4(2430)\Gamma \sim 100$ [see Table I and Eq. (7)], plotted against an $l(l+1)$ axis [or, equivalently, a $j(j+1)$ axis, since $l=j$ for these resonances]. Note the linearity of the curve in this representation, which indicates that these three resonances accurately obey the $l(l+1)$ energy interval rule of Eq. (5). The $l=0$ and $l=1$ levels in this p-p rotational band, which are the states at 2020 and 2060 MeV shown in Fig. 20, unfortunately lie below the 2082-MeV lower-energy limit of the Argonne C_{LL}, $\Delta\sigma_L$, and $\Delta\sigma_T$ measurements, and these levels have not been observed experimentally. However, we can use the $F-D=D-S$ equal-interval rule of Eq. (5) to extrapolate this curve to $l=0$, which gives an experimental p-p excitation energy of 143 MeV, or just the mass of a pion. This same excitation energy can be observed in the Λ-Λ dibaryon resonances of Fig. 21. An $E_{\rm rot}$ value of 20.6 MeV is obtained for this $pp\pi$ rotational band by averaging over the experimental G-F and F-D energy spacings; this value for $E_{\rm rot}$ is in excellent agreement with the values obtained from neighboring nonadiabatic rotational bands, as is shown in Figs. 18 and 19. The $^1F_3$ phase shift shown in Fig. 20 is the suggested assignment for an anomaly observed in the isotopic spin $I=0$ n-p amplitudes (Refs. 3 and 4) that closely matches the $I=1$ $^3F_3$ structure in the p-p amplitudes.

erated by these three resonances domonstrates that they do in fact accurately follow the energy interval rule that is expected for a nuclear rotational band.

Figure 20 illustrates another important fact; namely, that the expected $l=j=0$ and 1 levels in this p-p rotational band lie below the energy range of the Argonne C_{LL}, $\Delta\sigma_L$, and $\Delta\sigma_T$ measurements. The observed p-p resonances are very weak effects that persist only for short periods of time (as evidenced by their broad widths), and the C_{LL}, $\Delta\sigma_L$, and $\Delta\sigma_T$ data are crucially needed for their identification. But the measurements carried out at Argonne[1,38] have a lower momentum limit of 1.0 GeV/c in the laboratory frame of reference, which corresponds to a p-p center-of-mass energy of 2082 MeV; the extraplation of the p-p rotational band shown in Fig. 20 indicates that the $(l=j)$ $^1S_0$ and $^3P_1$ levels in this rotational band both occur at energies below 2082 MeV. Thus these two p-p resonances have not yet been delineated experimentally, so we must base our analysis of the p-p rotational band on the extrapolation procedure shown in Fig. 20.

By using the $F-D=D-S$ equal-energy interval rule to extrapolate the curve of Fig. 20 to $l=0$, we deduce that the S-state bandhead energy of the p-p diabaryon system is about 2020 MeV. Hence, since the mass of two unbound protons is 1877 MeV, we see that the p-p dibaryon excitation energy is about 143 MeV, or just the mass of a pion. Thus the Argonne $^1D_2$, $^3F_3$, and $^1G_4$ resonances accurately correspond to the $l=2$, 3, and 4 levels of a nonadiabatic rotational band in which the rotating bandhead is a virtual $pp\pi$ bound state. The rotational energy parameter for this p-p rotational band is $E_{\rm rot}=20.6$ MeV, as obtained by taking an average over the experimental $G-F$ and $F-D$ energy intervals. This is the $E_{\rm rot}$ value that is used in Figs. 18 and 19, and it can be seen to be in good agreement with the $E_{\rm rot}$ values of the neighboring nonadiabatic rotational bands, thus reinforcing this interpretation of the p-p resonances. If we substitute the values $E_0 \simeq 2020$ MeV and $E_{\rm rot} \simeq 20$ MeV into Eq. (5), we obtain calculated P, D, F, G, and H resonance energies of 2060, 2140, 2260, 2420, and 2620 MeV, respectively, as compared to the experimental energies of 2140, 2260, and 2430 MeV for the $^1D_2$, $^3F_3$, and $^1G_4$ resonances.

As further evidence for this interpretation of the p-p resonances, we note that other dibaryon resonances also exhibit this same virtual pion excitation mechanism. Figure 21 shows the strangeness $S=0$, -1, and -2 pp, $p\Lambda$, and $\Lambda\Lambda$ dibaryon excitations that have been reported to date.[26] As can be seen in Fig. 21, the $S=-2$ $\Lambda\Lambda$ dibaryon excitation accurately appears as a $\Lambda\Lambda\pi$ virtual bound state, thus echoing the $S=0$ $pp\pi$ virtual bound state that we deduced from the systematics of Fig. 20. The narrow-width $S=-1$ $p\Lambda$ dibaryon excitation, which

has been observed in a number of experiments,[26] appears as a $p\Lambda M$ excited state, where the excitation energy $M \sim 70$ MeV is just half of the excitation energy $\pi \sim 140$ MeV that occurs in the pp and $\Lambda\Lambda$ dibaryon resonances. A possible second $p\Lambda$ excitation level appears at an energy of roughly 140 MeV above the first $p\Lambda$ level in Fig. 21.

The occurrence of the π as a mass-shell (zero binding energy) excitation quantum has also been observed in a completely different hadronic system—the "charmed" D and D^* kaon system—as is demonstrated by the following strikingly similar decay modes[26]:

$$pp\pi(2020) \rightarrow pp(1877) + 143 \text{ MeV kinetic energy},$$
$$D^{*+}(2009) \rightarrow D^{+}(1868 + \pi^0(135) + 6 \text{ MeV kinetic energy}, \quad (8)$$
$$D^{*+}(2009) \rightarrow D^{+}(1868) + \gamma(141).$$

In the $pp\pi$ decay a virtual pion is transformed into kinetic energy, whereas in the D^* decays the pion is either emitted directly or else transformed into a photon.

We can summarize the results of the above discussion in the following statement: *The threshold for dinucleon resonance formation is equal to the threshold for pion production, and the excitation mechanism consists of the formation of a mass-shell $pp\pi$ virtual bound state, which is manifested experimentally in the form of a $pp\pi$ dinucleon rotational band.* It should be noted here that the identification of the three Argonne p-p resonances as the $l = 2$, 3, and 4 members of a nonadiabatic dinucleon rotational band is the only quantitative explanation which has been set forth to account for the existence of these three states. This p-p rotational band has the following properties:

(1) The p-p resonances have the broad widths ($\Gamma > 50$ MeV) that are expected[43] for rotational excitations (see Table I).

(2) The D, F, and G resonance energies accurately correspond to the nonadiabatic $l(l+1)$ interval rule of Eq. (5) [and also the general $j(j+1)$ interval rule of Eq. (4)].

(3) The extrapolation to $l = 0$ gives an S-state excitation energy of about 140 MeV (Fig. 20), which is a characteristic *hadronic* excitation unit [see Eq. (8)], and also a characteristic *dibaryon* excitation unit (see Fig. 21).

(4) The experimental moment of inertia of the rotating $pp\pi$ bandhead is consistent with the experimental moments of inertia of the neighboring nonadiabatic rotational bands (see Figs. 11 and 17–19).

There is one other piece of experimental information from the Argonne measurements that ties in with this concept of nonadiabatic dinucleon rotational bands. Preliminary Argonne experiments[3,4] show some structure in the n-p amplitudes. If this structure is interpreted in the context of an isotopic spin $I = 0$ resonance, then it indicates a mass, width, and inelasticity that closely resemble those of the $I = 1$ $^3F_3$ p-p resonance,[3] and its quantum numbers appear to be either $^1P_1$ or $^1F_3$. From the systematics of Eq. (5), $^3F_3$ and $^1F_3$ resonances, which are both $l = 3$ excitations, should appear at the same mass value (as we have indicated in Fig. 20). Thus the present results point to the quantum state assignment $^1F_3$ for this n-p structure, and it appears as the $I = 0$ counterpart of the dominant $I = 1$ $^3F_3$ enhancement in the p-p scattering amplitudes.

Although this proposed dinucleon rotational band meets the tests of properties (1)–(6) that we have de-

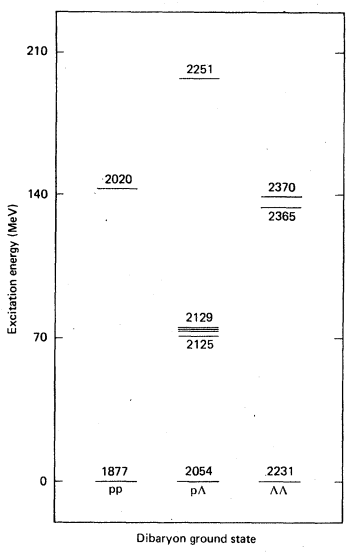

FIG. 21. The pp, $p\Lambda$, and $\Lambda\Lambda$ dibaryon resonances that have been observed experimentally, shown in the form of an energy level diagram. The $pp(2020)$ level in Fig. 21 is obtained from Fig. 20 of the present paper, and the $p\Lambda$ and $\Lambda\Lambda$ levels are from Ref. 26. Although the $\Lambda\Lambda(2365)$ and $\Lambda\Lambda(2370)$ dibaryon levels represent very weak experimental effects, it is interesting to note that they match the 140 MeV excitation energy of the pp dibaryon level. Of equal interest is the $p\Lambda(\sim 2127)$ dibaryon level shown in Fig. 21. This level has been observed in several experiments, and it has a very narrow width ($\Gamma \simeq 6$ MeV). The excitation energy for this level is about 70 MeV, which is just half of the excitation energy of the $pp(2020)$ and $\Lambda\Lambda(\sim 2367)$ levels. The weak $p\Lambda(2251)$ level in Fig. 21 appears roughly 140 MeV above the dominant $p\Lambda(\sim 2127)$ level. The main point we wish to bring out in Fig. 21 is that an excitation energy of 140 MeV for the pp dibaryon system is a result that fits in with other experimental dibaryon measurements, and hence lends additional credence to the systematics developed in Fig. 20.

scribed above, its existence raises several questions. Perhaps the most important of these has to do with the nonobservance of the S and P levels in the p-p rotational band. As we discussed in connection with Fig. 20, this results is attributable to the fact that the p-p S and P levels lie below the range of the important Argonne C_{LL}, $\Delta\sigma_L$, and $\Delta\sigma_T$ data. Thus the present analysis suggests the usefulness of extending the measurements at Argonne down from the existing laboratory momentum limit of 1.0 GeV/c to at least 800 MeV/c, which is the momentum that corresponds to the energy of the p-p S-state bandhead. It should be noted here in passing that the $pp\pi$ bandhead defined in Fig. 20 is a characteristic hadronic excitation—not a nuclear excitation—and some of the hadronic rotational bands have unobserved S states (see Figs. 14 and 15).

Another question about this dinucleon rotational band has to do with the $I=0$ resonances. If $I=1$ D, F, and G states exist, and if an $I=0$ F state also exists (see Fig. 20), then we might logically expect to find $I=0$ $^3D_2$ and $^3G_4$ enhancements appearing in the n-p amplitudes, and as yet there is no evidence for their existence. The answer to this question may involve the magnitudes of the $I=0$ cross sections. The $^3F_3$ resonance is the most prominent of the three observed $I=1$ enhancements, which suggests that the $^1F_3$ resonance is the most prominent $I=0$ enhancement. The n-p scattering matrix, which includes both $I=1$ and $I=0$ amplitudes, has much more parameter freedom than does the p-p scattering matrix, which includes only $I=1$ amplitudes. Thus $I=0$ resonance effects are intrinsically more difficult to observe than are $I=1$ resonance effects, and small $^3D_2$ and $^3G_4$ enhancements may be difficult to isolate experimentally.

A final question about the dinucleon rotational band has to do with the fact that a resonance is observed in the $^3F_3$ phase, but not in the $^3F_2$ or $^3F_4$ phases. The answer to this question involves two microscopic processes, both of which are essentially unknown: (1) the nuclear-force mechanism that leads to the production of a virtual pion in a p-p $^3F_3$ state, but (presumably) not in a $^3F_2$ or $^3F_4$ state and (2) the angular momentum quantization mechanism that produces resonances which have discrete angular momentum values. In connection with (2), it is worthwhile to point out that the identified $^1D_2$, $^3F_3$, and $^1G_4$ p-p resonances, and also the possible $^1F_3$ n-p resonance, are all states in which the (observed) orbital angular momentum is equal to the (observed) total angular momentum, i.e., these are states for which $l=J$. In highly nonadiabatic rotations the spin vector is essentially uncoupled from the orbital angular momentum vector,

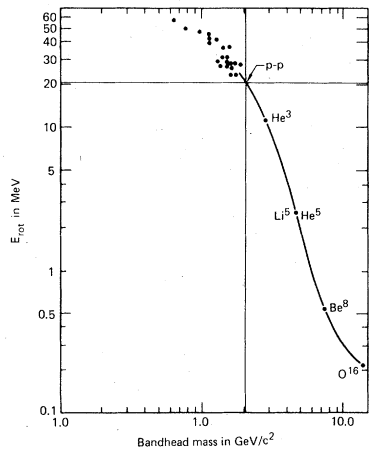

FIG. 22. A curve of experimental E_{rot} values for hadronic and nuclear rotational bands. This curve was drawn up (Ref. 52) prior to the discovery of the Argonne p-p resonances. As can be seen by the lines added to the drawing, the experimental E_{rot} value of 20.6 MeV for the p-p rotational band (Fig. 20) falls right on this pre-existing curve. This demonstrates the fact that the nonadiabatic hadronic and nuclear rotational bands described in the present paper were worked out in detail before the appearance of the Argonne p-p rotational band.

and it is possible that these observed $l=J$ enhancements reflect the nonadiabatic nature of the rotational motion rather than the nuclear force aspects of the pion production process. It has long been hoped that p-p and n-p inelastic-scattering experiments would provide vital clues as to the nature of the unknown pion-production mechanism, and it may be that the Argonne results are for the first time delineating an area of research that can give answers to this important question.

There is one final point to be mentioned here with respect to the present interpretation of the p-p and n-p resonances. The identification of nonadiabatic rotational bands in light nuclei and in baryon and meson excitations was completed and published[51] prior to the discovery of any of these Argonne nucleon-nucleon data anomalies. Thus the explanation that has been advanced in the present paper is *not* one that was specifically tailored to agree with the new Argonne data.[1] Figure 22 shows a curve of E_{rot} values for nonadiabatic rotational bands that was drawn up[52] before the present author had any information about the recent Argonne results. Superimposed on this figure is the p-p E_{rot} value of 20.6 MeV that we obtained from Fig. 20 of the present paper. As can be seen in Fig. 22, this subsequently deduced value of E_{rot} for the p-p rotational band is in accurate agreement with the pre-existing experimentally derived curve of E_{rot} values for rotations in hadrons and

in light atomic nuclei.

Although considerable uncertainties still exist in the analysis of the Argonne p-p and n-p data, it seems apparent from the results achieved thus far that the identified p-p resonances[1] serve as a direct and unique experimental link between the domains of nuclear physics and hadron physics. As stated in the abstract to this paper, the p-p rotational levels, which are nuclear in origin, can be used to pinpoint the mass of the p-p bandhead excitation, which is hadronic in origin.

ACKNOWLEDGMENTS

The author would like to acknowledge useful communications and discussions with A. Yokosawa and R. A. Arndt, and he would especially like to thank Professor Arndt for providing him with the results of a preliminary phase-shift analysis that includes the recent Argonne data. This work was performed under the auspices of the U. S. Department of Energy by the Lawrence Livermore Laboratory under Contract No. W-7405-ENG-48.

[1] I. P. Auer *et al.*, Phys. Rev. Lett. 41, 1436 (1978). Also see I. P. Auer *et al.*, *ibid.* 41, 354 (1978); Phys. Lett. 70B, 475 (1977); 67B, 113 (1977).

[2] K. Hidaka *et al.*, Phys. Lett. 70B, 479 (1977).

[3] A. Yokosawa (private communication); D. Underwood *et al.*, Bull. Am. Phys. Soc. 24, 636 (1979).

[4] H. Spinka, Argonne National Laboratory Report No. ANL-HEP-CP-78-56 (unpublished); A. Yokosawa, ANL Report No. ANL-HEP-CP-78-52 (unpublished).

[5] T. Kamae *et al.*, Phys. Rev. Lett. 38, 468 (1977); T. Kamae and T. Fujita, *ibid.* 38, 471 (1977).

[6] M. H. Mac Gregor *et al.*, Phys. Rev. 182, 1714 (1969).

[7] M. H. Mac Gregor, Phys. Rev. Lett. 42, 1724 (1979).

[8] M. H. Mac Gregor *et al.*, Phys. Rev. 169, 1149 (1968); 173, 1272 (1968).

[9] S. A. Moszkowski, *Handbüch der Physik* (Springer, Berlin, 1957), Vol. 34, pp. 413–550 (see pp. 497 and 498).

[10] Z. Szymanski, International Atomic Energy Agency (Vienna) Report No. IAEA-SMR 6/4, 1970 (unpublished), p. 97.

[11] See Eq. (36.3) in Ref. 9.

[12] A. Bohr and B. R. Mottelson, Phys. Rev. 89, 316 (1953); K. Dan. Vidensk. Selsk. Mat. Fys. Medd. 27, No. 16 (1953).

[13] J. P. Davidson, *Collective Models of the Nucleus* (Academic, New York, 1968).

[14] See p. 94 in Ref. 10.

[15] See p. 101 in Ref. 10.

[16] See, for example, A. K. Kerman, *Nuclear Physics*, edited by P. M. Endt and M. D. Emeur (North-Holland, Amsterdam, 1959), Chap. X.

[17] K. A. Erb and D. A. Bromley, Physics Today 32, No. 1, 34 (1979).

[18] The moment-of-inertia values shown in Fig. 1 were calculated from Fig. 2 of I. Y. Lee *et al.*, Phys. Rev. Lett. 38, 1454 (1976).

[19] This possibility is discussed by A. Bohr and B. R. Nottelson, *Nuclear Structure* (Benjamin, New York, 1975), Vol. 2, pp. 80 ff; Phys. Scr. 10A, 13 (1974).

[20] The experimental data for these low-mass rotational bands are taken from S. Fiarman and S. Hanna, Nucl. Phys. A251, 1 (1975); S. Fiarman and W. Meyerhof, *ibid.* A206, 1 (1973); F. Ajzenberg-Selove and T. Lauritsen, *ibid.* A227, 1 (1974); F. Ajzenberg-Selove, *ibid.* A248, 1 (1975); A268, 1 (1976); A281, 1 (1977); A300, 1 (1978); P. M. Endt and C. Van Der Leun, *ibid.* A310, 1 (1978).

[21] J. M. Eisenberg and W. Greiner, *Nuclear Models* (North-Holland, Amsterdam, 1975), pp. 26–28.

[22] Figure 2 is taken from Fig. 2 of N. Cindro *et al.*, Phys. Rev. Lett. 39, 1135 (1977).

[23] M. H. Mac Gregor, *The Nature of the Elementary Particle* (Springer, New York, 1978), Table 12.1 on p. 171. Also see Table XXX in Ref. 32.

[24] H. Friedrich *et al.*, Phys. Lett. 36B, 189 (1971); R. C. Fuller, *ibid.* 43B, 445 (1973).

[25] The four rotational levels in ^{20}Ne are brought out in Fig. 11 of F. Ajzenberg-Selove, Nucl. Phys. A300, 1 (1978).

[26] Particle Data Group, Review of Particle Properties, Phys. Lett. 75B, 1 (1978).

[27] S. Fiarman and S. Hanna, Nucl. Phys. A251, 1 (1975).

[28] See the discussion in Ref. 153 of Ref. 32.

[29] C. C. Chang *et al.*, Phys. Rev. Lett. 29, 307 (1972); also see A. Niiler *et al.*, Phys. Rev. C 1, 1342 (1970).

[30] J. Arvieux, Nucl. Phys. A221, 253 (1974).

[31] M. H. Mac Gregor, Lett. Nuovo Cimento 1, 427 (1971).

[32] M. H. Mac Gregor, Phys. Rev. D 9, 1259 (1974).

[33] See Chaps. 15 and 16 and Appendix H in Ref. 23.

[34] T. Hirose *et al.*, Nuovo Cimento 50A, 120 (1979). Although the quantum numbers of this resonance have not been determined, its narrow width ($\Gamma < 67$ MeV) singles it out as a rotationless excitation. As these authors point out, this new resonance does not fit in with the conventional $q\bar{q}$ quark model states.

[35] See Table 15.2 on p. 238 of Ref. 23.

[36] M. H. Mac Gregor *et al.*, Annu. Rev. Nucl. Sci. 10, 291 (1960).

[37] R. A. Arndt, Phys. Rev. 165, 1834 (1968). Also see S. Furuichi *et al.*, Nuovo Cimento 23A, 375 (1974); H. Suzuki, Prog. Theor. Phys. 50, 1080 (1973); 54, 143 (1975); S. Furuichi and H. Suzuki, *ibid.* 57, 1803 (1977).

[38] W. de Boer *et al.*, Phys. Rev. Lett. 34, 558 (1975). Also see E. K. Biegert *et al.*, Phys. Lett. 73B, 235 (1978).

[39] See the last three references in Ref. 1.

[40] See the first and third references in Ref. 1.

[41] K. Hidaka, Argonne National Laboratory Report No. ANL-HEP-CP-78-15 (unpublished).

[42] N. Hoshizaki, Prog. Theor. Phys. 60, 1796 (1978); 61, 129 (1979).

[43] See Figs 12.1 and 12.2 on p. 160 of Ref. 23.

[44] N. Hoshizaki, Prog. Theor. Phys. 58, 716 (1977).

[45] W. Grein and P. Kroll, Nucl. Phys. B137, 173 (1978); P. Kroll, University of Wuppertal Reports Nos. WU-B-78-13 and WU-B-78-30 (unpublished).

[46]R. A. Arndt (private communication).
[47]G. L. Kane and G. H. Thomas, Phys. Rev. D 13, 2944 (1976); D. D. Brayshaw, Phys. Rev. Lett. 37, 1329 (1976); S. Minami, Phys. Lett. 74B, 120 (1978); S. Furuichi *et al.*, Prog. Theor. Phys. 61, 1127 (1979).
[48]E. L. Berger *et al.*, Argonne National Laboratory Report No. ANL-HEP-75-72 (unpublished); G. H. Thomas, ANL-HEP-77-75 (unpublished).
[49]W. M. Kloet *et al.*, Phys. Rev. Lett. 39, 1643 (1977).
[50]M. Arik and P. G. Williams, Nucl. Phys. B136, 425 (1978).
[51]See Sec. IX, Figs. 10–12, and Table XXX in Ref. 32.
[52]See Fig. 16.6 on p. 271 of Ref. 23.